2013

Aβ Alters the DNA Methylation Status of Cell-fate Genes in an Alzheimer's Disease Model

Gary D. Isaacs
Liberty University, gdisaacs@liberty.edu

Noor Taher

Courtney McKenzie

Rebecca Garrett

Matthew Baker

See next page for additional authors

Aβ Alters the DNA Methylation Status of Cell-fate Genes in an Alzheimer's Disease Model

Noor Taher[a], Courtney McKenzie[a*], Rebecca Garrett[a*], Matthew Baker[a*], Nena Fox[b], and Gary D. Isaacs[a].

[a]Department of Biology and Chemistry, Liberty University, Lynchburg, VA 24502

[b]University of Virginia School of Medicine, Tissue Culture Facility, Charlottesville, VA 22908

[*]Authors contributed equally to this work.

Correspondence should be made to: Gary

D. Isaacs, Ph.D.

1971 University Boulevard

Lynchburg, VA 24502

Tel: (434) 582-2224

Fax: (434) 582-2488

E-mail: gdisaacs@liberty.edu

Reprinted from *Journal of Alzheimer's Disease*, Volume 38, Number 4. Noor Taher, Courtney McKenzie, Rebecca Garrett, Matthew Baker, Nena Fox, and Gary D. Isaacs. "Amyloid-β Alters the DNA Methylation Status of Cell-fate Genes in an Alzheimer's Disease Model." Copyright 2013, with permission from IOS Press.

IOS Press: www.iospress.nl.
Journal of Alzheimer's Disease: http://www.iospress.nl/journal/journal-of-alzheimers-disease/.

Abstract

Alzheimer's disease (AD) is characterized by neurofibrillary tangles and extracellular amyloid-β plaques (Aβ). Despite ongoing research, some ambiguity remains surrounding the role of Aβ in the pathogenesis of this neurodegenerative disease. While several studies have focused on the mutations associated with AD, our understanding of the epigenetic contributions to the disease remains less clear. To that end, we determined the changes in DNA methylation in differentiated human neurons with and without Aβ treatment. We isolated the DNA from neurons treated with Aβ or vehicle, and digested the two samples with either a methylation-sensitive (HpaII) or a methylation-insensitive (MspI) restriction endonuclease. The fragments were amplified and co-hybridized to a commercial promoter microarray. Data analysis revealed a subset of genomic loci that shows a significant change in DNA methylation following Aβ treatment in comparison to the control group. After mapping these loci to nearby genes, we discovered high enrichment for cell-fate genes that control apoptosis and neuronal differentiation. Finally, we incorporated three of those genes in a possible model suggesting the means by which Aβ contributes to the brain shrinkage and memory loss seen in AD.

Keywords: Alzheimer's disease, DNA methylation, beta amyloid fragment (1-40), neurogenesis

Introduction

Several lines of evidence suggest that epigenetic modifications, like DNA methylation, play a role in AD. First, late onset Alzheimer's disease, which represents over 90% of AD cases, appears sporadic in nature with no known genetic cause [1]. Consistent with this, the inheritance pattern of AD in monozygotic twins suggests a non-Mendelian mode of acquiring the disease [2-4], indicating that DNA sequence alone does not explain AD development. Second, evidence of a parent-of-origin effect has been described for AD, identifying several genomic regions that are transmitted through the maternal line to affected individuals [5]. The requirement of an environmental contribution (in this case being the maternal germ line) is consistent with an epigenetic mechanism [6]. It is interesting to note that one of the most common mechanisms of parent-of-origin effects is "genomic imprinting" mediated by DNA methylation [7]. Third, studies in mice and humans suggest a global change in DNA methylation when comparing AD subjects to their control counterparts. In humans, monozygotic twins discordant for AD displayed differential DNA methylation levels in the anterior temporal neocortex, a region severely affected in AD [8]. The regions of the brain not affected by AD displayed identical DNA methylation levels, demonstrating the specificity of this result. The specific reduction of DNA methylation in the AD twin may provide a rationale for the link between folate deficiency and AD, since one of the normal functions of folate is to donate methyl groups for DNA methylation reactions [9]. Finally, the expression levels of several AD-associated genes (APP, β-APP cleaving enzyme, and neprylisin) are regulated based on the DNA methylation status of their respective promoters [10, 11]. It is important to note that although AD is associated with a global hypomethylation of the genome, the neprylisin (NEP) promoter actually becomes hypermethylated in murine cerebral endothelial cells treated with Aβ [11]. This evidence

demonstrates that a gene can be affected by an epigenetic change that increases or decreases its normal methylated state. NEP expression is significantly reduced in AD brains, most likely due to methylation-dependent silencing [11, 12]. Taken together, these data strongly suggest that DNA methylation plays a key role in the development of AD.

The identification of epigenetic marks associated with AD development would provide excellent diagnostic markers for mapping AD progression and propose a novel, epigenetic model to how AD initially begins. In addition, a non-mutational, reversible process like DNA methylation would be vulnerable to the development of epigenetic therapeutics aimed at preventing or even undoing age-related changes to the genome.

In order to determine if DNA methylation plays a role in AD, human IMR-32 cells were differentiated into mature neuronal cells and treated with Aβ. The methylation pattern of individual genomic regions was analyzed using genome-wide promoter arrays. Comparison of the methylation patterns before and after treatment identified the specific epigenetic changes that occur as neuronal development progresses toward an AD-like state.

Several methods have been described for detection of the presence of methylated DNA. Bisulfite sequencing [13] utilizes the chemical differences between methylated and unmethylated cytosine. Sodium bisulfite reacts with normal cytosine (unmethylated) to form an intermediate easily deaminated to uracil. Sequencing will reveal a thymine at locations corresponding to unmethylated cytosines. Conversely, methylated cytosines are protected from the chemical transition to uracil, so no changes in the base sequence are detected (see [14] for review). Although reliable, this method is not easily adapted to meet the requirements of a genomic-sized examination since sequencing at this scale is quite expensive.

The methylated DNA immunoprecipitation (MeDIP) method [15] uses an antibody to capture DNA fragments by way of their methylated cytosines. The capture of specific regions is expressed as a purification enrichment and can be determined using PCR or by hybridizing the material to genomic chip arrays. The latter platform allows the global determination of methylated regions. Because this method does not detect unmethylated cytosines, a failure to detect a CpG region of interest could be due to its hypomethylated state or a technique problem in the purification process.

Other methods of DNA methylation determination utilize the specificity of restriction endonucleases for a particular CpG methylation state (methylation-sensitive restriction enzyme; MSRE) followed by PCR analysis. An example of an MSRE is HhaI, which recognizes and cuts 5'-GCGC-3' sequences only when they are unmethylated [16]. PCR of the region will produce a visible product only when the included CpG is methylated and thus protected from enzymatic digestion. This assay requires additional PCR controls to determine if failed PCR runs are due to poor primer design or a truly hypomethylated region.

This short coming can be resolved when two MSREs with different methylation sensitivities are used. For example, HpaII and MspI are isoschizomers that both recognize 5'-CCGG-3' sequences. HpaII digestion is blocked when these sequences are methylated, while MspI is insensitive to the methylation status of the recognition site. When these fragments are cohybridized to genomic microarrays (described as **H**paII tiny fragment **E**nrichment by **L**igation-mediated **P**CR; or HELP assay), intergenomic and intragenomic comparisons concerning DNA methylation can be made [17]. Because this method can detect methylated and unmethylated regions on a genomic scale, the HELP assay was the method of choice for this study.

Methods and Methods

Cell Culture

Cholinergic IMR-32 human neuroblastoma cells [18] (ATCC) were grown and differentiated as previously described [19]. The cells were maintained in culture in proliferation medium [MEM with NEAA (Invitrogen 10370-0210, 2mM L-glutamine, 1mM sodium pyruvate, 10% FCS] at 37°C in an atmosphere of 5% CO_2. The cells were plated at a density of 5×10^5 cells/15 cm plate and grown for 48 hours in this proliferation media. The proliferation media was then replaced by differentiation media (proliferation medium with 2% FCS and 2mM sodium butyrate). The cells were maintained in differentiation media for 7 days then treated with either 25 µM $A\beta_{1\text{-}40}$ peptide (Invitrogen 03-136) (prepared as described previously [11]) or vehicle for 48 hours. The cells were then rinsed with cold PBS (phosphate-buffered saline), harvested by scraping, pelleted by centrifugation in 1.5 ml Eppendorf tubes, and stored at -80°C.

DNA Isolation and Digestion

The undifferentiated, differentiated, and Aβ-treated cell pellets were thawed and kept on ice until they were treated with 478 µl of lysis buffer (0.5% SDS, 0.2M NaCl, 20mM EDTA), 20 µl protease K (2.5 mg/ml), and 2 µl RNase (10mg/ml). The reagents were mixed with the pellets by gentle agitation, and the tubes were incubated in a 42°C water bath overnight. Each sample was treated with 500 µl of phenol-chloroform-isoamyl alcohol (PCIAA) and incubated on a rotary wheel for 10 minutes at 37°C. The samples were then separated into an organic and aqueous layer by centrifuging at 17,000×g for 5 minutes. The aqueous layer containing the DNA in each sample was transferred to a new 1.5 ml Eppendorf tube. This process was repeated once to ensure DNA purity. To precipitate the DNA, 3× the sample volume in 100% ethanol was added to each sample, along with 1/10 the sample volume in 3M sodium acetate and .5 µl of glycogen

(20 mg/ml). The samples were then centrifuged at 17,000×g for 1 hour. The supernatant was removed, and the pellets were subsequently washed gently with 70% ethanol. The pellets were finally resuspended in 200 µl of deionized water. The DNA in each sample was then quantified using UV spectroscopy.

Each sample was digested with HpaII and MspI in separate reactions according to the manufacturer's recommendations. Each reaction contained 1 µg of DNA and either 4 µl of HpaII (10,000 U/ml) or 2 µl of MspI (20,000 U/ml) (New England Biolabs). The reactions were brought to a final volume of 200 µl with deionized water and incubated overnight at 37°C. The DNA from each sample was then purified as described above and resuspended in 15.5 µl of 10 mM Tris-HCl (pH 8).

Ligation-mediated PCR

To avoid degradation or re-annealing of the overhangs, the ligation was performed immediately after the digestion. Two sets of adapters were used: NHpaII12 (5'-CGGCTTCCCTCG-3'), NHpaII24 (5'-GCAACTGTGCTATCCGAGGGAAGC-3'), JHpaII12 (5'-CGGCTGTTCATG-3'), JHpaII24 (5'-CGACGTCGACTATCCATGAACAGC-3'). The 24-mer and 12-mer oligonucleotides of each set were annealed together in preparation for the ligation. Ligation was performed on HpaII and MspI-digested undifferentiated DNA, differentiated DNA, and Aβ DNA. Reactions were carried out in PCR tubes and consisted of 6 µl of 5× T4 ligase buffer (Invitrogen), 15.5 µl digested DNA, 4 µl of 50 µM pre-annealed JHpaII linkers, 4 µl of 50 µM pre-annealed NHpaII linkers, and 1 µl of T4 DNA ligase (4 U/µl). The reactions were put in a thermocycler at 16°C overnight. The reactions were then diluted to 10 ml by 10 mM Tris-HCl (pH 8).

The LM-PCR reactions contained 5 µl of HpaII-digested DNA or 2.5 µl of MspI-digested DNA, .5 µl of 100 µM JHpaII24 primer, .5 µl of 100 µM NHpaII24 primer, 25 µl of 2× SsoFast EvaGreen qPCR Supermix (Bio-Rad), and were brought to a final volume of 50 µl with deionized water. The MspI-digested DNA used in the amplification was half the volume of the HpaII-digested DNA. This is due to the difference in complexity of fragments in the MspI-digested DNA, which will cause these fragments to amplify and saturate the solution in the PCR faster and undergo "extra" cycles without amplification. This makes the sample susceptible to unwanted artifacts. The issue was circumvented by using half as much MspI-digested DNA as HpaII-digested DNA as was previously reported [17]. The LM-PCR scheme began with an initial extension step at 72°C for 10 minutes, 15-20 cycles of 95°C for 30 seconds and 72°C for 3 minutes, and a final extension step at 72°C for 10 minutes. The reactions were purified using Qiagen's QIAquick PCR Purification Kit (50) according to the manufacturer's instructions, and DNA was quantified using UV spectroscopy.

DNA microarrays and data analysis

Five 385K DNA Methylation microarrays were purchased from Roche NimbleGen to hybridize 2 undifferentiated DNA samples, 2 differentiated DNA samples, and 1 DNA sample from differentiated cells treated with Aβ. All samples were amplified by LM-PCR and purified to produce at least 4 µg of DNA with a concentration of at least 250 ng/µl.

The raw microarray data from Roche NimbleGen was processed using Matlab 2011. First, correlation graphs were generated to examine the relationship between the 2 undifferentiated DNA microarrays and between the 2 differentiated DNA microarrays. Each array contained 4,288 random probes designed by Roche NimbleGen for control purposes. The background fluorescence threshold was taken as 2.5 mean absolute deviations (MAD) above the

median fluorescence signal of the random probes [20, 21]. For a probe to be considered valid, the probe intensity from the MspI sample had to be above the threshold in all 5 arrays. An HpaII/MspI ratio histogram was generated for each condition (undifferentiated, differentiated, and Aβ-treated). The undifferentiated and differentiated data were an average of 2 microarray data sets for those conditions. All histograms were mean-centered, and the x-axis was converted from linear scale to $\log_2$.

QPCR

Site-specific qPCR confirmations were used to validate the microarray data and show their biological significance. DNA from IMR-32 cells was digested with HpaII and MspI in separate reactions as described above. An "uncut" control was included to serve as a positive control for maximum amplification possible. The recipe for the uncut digestion reaction was identical to that of MspI, except that 2 µl of 50% glycerol were added instead of the enzyme. The samples were subsequently purified as previously described and resuspended in 200 µl of deionized water.

Primers were designed around the closest 5'-CCGG-3' to a given probe using Primer3 (http://frodo.wi.mit.edu/). The PCR product size range was chosen to be between 80-140 bp, the primer T_m was 60±2ºC, and the primer size was 20±2 bp. All other criteria were left as the default settings by the software. The 25 µl qPCR reactions contained .015-.025 µg of template DNA, 12.5 µl of 2x Supermix, and forward and reverse primers with a final concentration of .625 µM each. Reactions lacking DNA template were also included as control for primer self-annealing and amplification. Amplification was performed using a BioRad MJ Mini Personal Thermal Cycler. The touchdown qPCR scheme began with an initial melting step at 95°C for 5 minutes. The first cycle was repeated 19 times and consisted of a melting step at 94°C for 10 seconds, annealing step at 69°C for 30 seconds, and a final extension step at 72°C for 30

seconds. The annealing step decreased by 0.5°C each cycle. The second cycle followed immediately and consisted of a melting step at 94°C for 10 seconds, annealing at 59°C for 30 seconds, and an extension step at 72°C for 30 seconds. This second cycle was repeated 24 times with a constant annealing temperature and was followed by a final extension step at 72°C for 5 minutes. The amplification graphs were generated by BioRad CFX Manager 2.0. The quantification cycle (Cq) values were obtained for all samples and used for quantitation.

Gene Ontology

Gene symbols were linked to the 222 most changing regions (111 regions becoming hypomethylated and 111 regions becoming hypermethylated following Aβ treatment) using GREAT, a region/gene association and annotation software developed by Stanford University and Bejarano Lab [22]. Human genome 18 build was used for the species assembly, and the whole genome was used as the reference list. The resulting gene symbols were analyzed by GeneCodis, a gene annotation website for ontological assignments [23-25]. The gene symbols from three methylation categories (regions becoming hypomethylated, hypermethylated, and a random list) were analyzed using the following GeneCodis criteria: level 7 (the most stringent), a minimum of 3 genes associated with that ontology, and a chi-square value that was lower than the lowest obtained chi square value from the random list. The enrichment value from which the chi-square value was calculated by dividing the ratio of genes for a gene ontology in the list to the total number of genes in the list by the ratio of genes for that gene ontology in the genome to the total number of genes in the genome.

$$\frac{\dfrac{\text{Number of Genes for G.O. in List}}{\text{Number of Genes in List}}}{\dfrac{\text{Total Number of Genes for G.O.}}{\text{Total Number of Genes in Genome}}}$$

Results

Global DNA Methylation Levels Remain Largely Unchanged After Aβ Treatment.

In order to determine if DNA methylation plays a role in the development of AD, we set out to identify the methylation status of neurons before and after Aβ treatment. We utilized a microarray-based technique, known as the HELP assay, which compares the endonuclease efficiency of a methylation-sensitive enzyme (HpaII) versus a methylation-insensitive enzyme (MspI). These enzymes are isoschizomers that cleave the same 5'-CCGG-3' palindrome. This recognition sequence contains a CpG dinucleotide that can serve as the target for *de novo* methylation by the DNMT3 family of methyltransferases.

Analysis of the HpaII/MspI ratios before and after Aβ treatment revealed a bi-modal distribution of DNA methylation levels (Figure 1). In general, this distribution pattern represented groups of ratios that were hypermethylated or hypomethylated relative to the mean of all the ratios. Approximately 72.8% of the control ratios fell in the lower distribution (representing the high methylation fraction), while only 27.2% of the control ratios fell in the higher distribution (representing the low methylation fraction) (Figure 1A). A similar pattern was observed after Aβ treatment, with hypermethylated and hypomethylated fractions being 71.8% and 28.2% of the ratios, respectively (Figure 1B). The correlation of the control and Aβ -treated ratios was 0.978 (Figure 1B inset), demonstrating the global similarity of these samples. Interestingly, this correlation was slightly higher than the correlation between two independent control microarray samples (R = 0.9475; Supplemental Figure 1), indicating a higher variability in the control replicates than in the control to Aβ comparison. Overall, the Aβ treatment had no significant effects on the global DNA methylation levels in the neuronal cells.

Site-specific qPCR Confirms the Microarray Data.

We then analyzed specific loci within our microarray data to determine if we could detect discrete levels of DNA methylation as indicated by the microarray data. For this purpose, we randomly chose genomic regions from the microarray dataset to examine the specific HpaII sensitivity by quantitative PCR. We chose regions that contained $\log_2$ HpaII/MspI ratios less than the mean for the hypermethylated distributions in order to detect high methylation levels (refer to Figure 1 - blue curves). We also chose regions that contained $\log_2$ HpaII/MspI ratios greater than the mean of the hypomethylated distributions to detect lower levels of DNA methylation (Figure 1 - red curves). We then mapped all the 5'-CCGG-3' sequences within the regions in order to design PCR primers to amplify across select restriction sites. Some regions only contained one restriction site (Figure 2A), while others contained many (Figure 2B and C). When we performed qPCR analysis of these particular 5'-CCGG-3' sequences, we found that the site-specific results were aligned with the microarray data (Figure 2E-H). For example, two hypomethylated regions were chosen, ChrY:14100892 and Chr4:122212661 (Figure 2A and C), because they contained probes with $\log_2$ values greater than the average of the hypomethylation distribution in Figure 1A and B, respectively. QPCR analysis of a restriction site in these regions demonstrated low levels of amplification in the HpaII samples (Figure E and G). This indicates that HpaII is efficiently cutting these CpG-containing sequences; therefore, these sequences must not be heavily methylated. Since MspI can cut its restriction site regardless of CpG methylation, qPCR amplification of MspI-treated DNA should always be low and serves as a negative control. Two hypermethylated regions were also chosen, Chr16:67328870 and Chr15:94698105 (Figure 2B and D), because they contained probes with $\log_2$ values below the average of the hypermethylation distribution in Figure 1A and B, respectively. QPCR analysis of these regions

demonstrated much higher levels of amplification in the HpaII samples relative to the MspI controls (Figure 2F and H). This indicates that HpaII is relatively inefficient at cleaving these sites; therefore, these sequences must contain significant levels of DNA methylation. Taken together, our qPCR-based approach can determine sequence-specific DNA methylation levels that are consistent with the microarray-based data.

Aβ Induces Significant Changes in DNA Methylation at a Subset of Genomic Locations. Since Aβ treatment did not affect neuronal DNA methylation levels on a global scale, we decided to focus our qPCR approach on the specific genomic loci that contained a significant change in their epigenetic ratio in relation to Aβ treatment. To this end, we subtracted the control microarray data from the Aβ-treated microarray data and plotted the $\log_2$ ratios as a histogram (Figure 3A). Ratios greater than zero indicated probes that were more hypomethylated in the Aβ condition, while ratios less than zero indicated probes that were more hypermethylated in the Aβ condition. Although the resulting data further demonstrates the similarity between the two datasets (85% of the data are within 1 STD), some regions of major change can be seen at the extremes of the plot (Figure 3B and C). These specific regions were of the greatest interest to us, since they represented significant epigenetic alterations as a result of Aβ treatment. We decided to focus our attention on these regions of greatest absolute change defined as the top 0.1% of all changing ratios (0.05% gaining methylation; 0.05% losing methylation). This translated into 111 probes that gained methylation and 111 probes that lost methylation as neurons were exposed to Aβ, and corresponded to probe ratios exceeding 3 standard deviations from the average change of all probes.

We decided to use our qPCR approach to test if, in fact, we could predict the methylation change at specific 5'-CCGG-3' sequences based on the microarray data. We randomly chose 12

genomic regions from each 111 probe list and designed qPCR primers for two 5'-CCGG-3' sequences in each region (named 'upstream' and 'downstream' in relation to the highest changing probe). As expected, microarray regions that gain methylation in the Aβ condition (Figure 4A and C; negative bars) contain 5'-CCGG-3' sequences that are more difficult to cleave with HpaII when analyzed by qPCR (Figure 4B and D). Likewise, microarray regions that lose methylation in the Aβ condition (Figure 4E and G; positive bars) contain sequences that are more easily cleaved by HpaII when analyzed by qPCR (Figure 4F and H). Of all the 5'-CCGG-3' loci tested, over 97% confirmed the microarray results (44 out of 45; Supplemental Figures 2 and 3). QPCR results from only 45 5'-CCGG-3' loci of the 48 examined were kept since qPCR data from 3 regions contained bad primer pairs as indicated by their melting curves. It is interesting to note that both CpGs tested in a given region gave a similar result. This indicates that the methylation changes that occurred within a particular genomic region were not limited to a particular 5'-CCGG-3' sequence, but rather were indicative of several other loci in the region as well. This is consistent with previous work that demonstrates the spreading of epigenetic marks and explains the similarity in our independent qPCR analyses within a region (i.e., the upstream and downstream qPCR results).

Gene Ontology of Aβ-induced Epigenetic Changes Implicates Cell-Fate Pathways.

We next wanted to determine if any of the regions that significantly change their DNA methylation status (i.e., increase methylation or decrease methylation) were associated with a particular cellular process. For this purpose, the genomic regions were mapped to the nearest transcription start site (TSS) using GREAT (http://bejerano.stanford.edu/great/public/html). Once duplicate gene symbols obtained from this software were removed, ontological assignments were determined using GeneCodis (http://genecodis.cnb.csic.es). Regions that lost

DNA methylation as a result of Aβ exposure were found near genes associated with neurogenesis, neuronal differentiation/development, and the negative regulation of apoptosis (Table 1). Regions that gained DNA methylation as a result of Aβ exposure were also found near genes associated with neurogenesis and apoptosis. These cellular pathways were specifically enriched in our Aβ-induced change lists, since a randomly generated gene list of similar size failed to produce ontological assignments with similar p-values.

While some epigenetic changes were located over 10kb from the nearest TSS (e.g., DLX1), other changes were located at the promoter region (e.g., VHL). While DLX1 was identified because of a distal epigenetic change downstream of its TSS, it is interesting to note that it also contained a similar change proximal to its TSS, though the degree of change was not as great (Figure 5). Since our microarrays primarily focused on promoter proximal regions, it is not surprising that many epigenetic changes were found near genes (Supplemental Table 1). Of the regions that lost methylation, 45% were located within 5 kb from the nearest TSS, while only 16% of the regions that gained methylation were in this promoter-proximal window (Supplemental Figure 4). Although this may indicate different mechanisms of epigenetic control, future genomic studies that do not contain a promoter bias will determine if Aβ-induced methylation changes have a preference for loci based on their distance from transcription start sites.

As a whole, these results support the idea that AD pathology is produced, in part, by the epigenetic changes that occur within neurons as they age or are exposed to Aβ deposits. Although it is not known if these changes cause AD or are merely a result of AD progression, we believe these data further define AD as an epigenetic disease with specific cellular processes affected by altered methylation.

Discussion

We can make three conclusions from the results presented herein. First, Aβ treatment of differentiated neurons *in vitro* does not change the global DNA methylation levels of the genome. There is an overall consistency in the distribution of methylation levels between the control sample and Aβ sample microarrays accompanied by a high correlation in probe values between these conditions. Second, exposure to Aβ leads to significant changes in methylation at a subset of loci, while others remain largely unchanged. Third, these significantly changing loci are associated with genes involved in neuronal differentiation, neurogenesis, and apoptosis control. Therefore, Aβ may contribute epigenetically to AD progression by propagating neuronal loss of function and death. This is quite significant since epigenetic modifications are reversible and might provide an avenue for the future treatment of AD. These modifications might also provide an epigenetic signature, indicative of the early genomic changes associated with AD.

After mapping the microarray regions showing significant changes in methylation to nearby genes, we found that some regions were 70-300 bp away from the nearest genes, while others were more than 150,000 bp away. Although some of those regions are fairly distant from the nearest TSS, it is well-established that gene regulation can proceed distally through enhancer mechanisms (see [26, 27] for review). With this in mind, it would be interesting to determine if these distal changes actually define enhancer regions. It is also important to note that GREAT software maps input loci to the closest “canonical” TSS of a given gene, potentially ignoring closer TSS sites. In other words, some of the regions in our data may be closer to a nearby gene than the results seem to suggest.

It is also important to utilize a better model for studying Aβ pathology, as a cancer-based model such as ours can introduce a background of methylation levels/patterns foreign to normal cells. For example, the hypomethylation peak seen in genome-wide DNA methylation profiles in

Figure 1A and B may be a remnant of the cancerous IMR-32 cell line from which our neurons were differentiated. This relatively large portion of genomic hypomethylation may be the result of long repetitive sequences becoming hypomethylated with cancer progression [28-30]. Current pilot studies using a mouse model system demonstrate a uniform distribution of methylation patterns, adding credibility to this hypothesis. Therefore, we expect future non-cancer based models to lack such a hypomethylated peak and be even more indicative of what occurs in an AD brain.

Given the high enrichment in our gene ontology for cell-fate genes, we developed a coherent model outlining how Aβ possibly contributes to AD pathology by manipulating three such genes: DLX1, VHL, and PCNT. Previous work by Cobos et. al. shed light on the involvement of DLX transcription factors on the migration and differentiation of GABAergic interneurons [31]. Interestingly, they observed disruption in migration patterns and premature increase in neurite growth in interneurons of DLX1/2 double mutant mice. Their results demonstrated the importance of DLX1 and DLX2 in repressing neurite growth and maintaining a compact cell shape necessary for migration maneuvers. VHL, on the other hand, is a known tumor suppressor that is mutated in some neoplasms (see [32] for review). The third gene of interest, PCNT, is known for its involvement in the correct spindle assembly and metaphase progression during mitosis [33, 34], and some mutations in PCNT are associated with microcephaly [35]. Keeping in mind that Aβ causes significant hypomethylation of DLX1 and VHL and hypermethylation of PCNT as we saw, it is possible to suggest that Aβ promotes “de-differentiation” of normal neurons and prevents neuronal precursor cells from dividing and replacing the damaged cells (Figure 6). Such effects may contribute to the memory loss and aberrant brain morphology seen in AD. However, we present this model with some reservations;

although DNA methylation and demethylation have been traditionally associated with transcriptional repression and activation, respectively, some important exceptions have been reported [36-39]. Therefore, without mRNA transcription data, this model requires further support.

Future studies utilizing *in vivo* models coupled with expression data will further clarify the effects of Aβ on neurons by monitoring the outcomes of differentially methylated genes. Hydroxymethylation is another emerging and interesting epigenetic modification that can possibly contribute to disease progression. Such experiments can focus on genes associated with differentiation and tumor suppression (such as DLX1 and VHL) and, in addition, evaluate the candidacy of Aβ-affected regions far apart from TSSs as distal enhancer regions. Combined with these efforts to confirm and supplement, our study promotes further exploration of AD from an epigenetic point of view.

Acknowledgements

This work was supported by the Jeffress Memorial Trust Award (Grant #J-998), Virginia Academy of Science, and Liberty University. We would like to thank Rebecca Haraf for critical reading of this manuscript.

References

[1] Zawia NH, Lahiri DK, Cardozo-Pelaez F (2009) Epigenetics, oxidative stress, and Alzheimer disease. *Free Radic Biol Med* **46**, 1241-1249.

[2] Gatz M, Pedersen NL, Berg S, Johansson B, Johansson K, Mortimer JA, Posner SF, Viitanen M, Winblad B, Ahlbom A (1997) Heritability for Alzheimer's disease: the study of dementia in Swedish twins. *J Gerontol A Biol Sci Med Sci* **52**, M117-125.

[3] Gatz M, Fratiglioni L, Johansson B, Berg S, Mortimer JA, Reynolds CA, Fiske A, Pedersen NL (2005) Complete ascertainment of dementia in the Swedish Twin Registry: the HARMONY study. *Neurobiol Aging* **26**, 439-447.

[4] Raiha I, Kaprio J, Koskenvuo M, Rajala T, Sourander L (1997) Alzheimer's disease in twins. *Biomed Pharmacother* **51**, 101-104.

[5] Bassett SS, Avramopoulos D, Fallin D (2002) Evidence for parent of origin effect in late-onset Alzheimer disease. *Am J Med Genet* **114**, 679-686.

[6] Liu L, Li Y, Tollefsbol TO (2008) Gene-environment interactions and epigenetic basis of human diseases. *Curr Issues Mol Biol* **10**, 25-36.

[7] Hall JG (1990) Genomic imprinting: review and relevance to human diseases. *Am J Hum Genet* **46**, 857-873.

[8] Mastroeni D, McKee A, Grover A, Rogers J, Coleman PD (2009) Epigenetic differences in cortical neurons from a pair of monozygotic twins discordant for Alzheimer's disease. *PLoS One* **4**, e6617.

[9] Ravaglia G, Forti P, Maioli F, Martelli M, Servadei L, Brunetti N, Porcellini E, Licastro F (2005) Homocysteine and folate as risk factors for dementia and Alzheimer disease. *Am J Clin Nutr* **82**, 636-643.

[10] Cacabelos R (2008) Pharmacogenomics in Alzheimer's disease. *Methods Mol Biol* **448**, 213-357.

[11] Chen KL, Wang SS, Yang YY, Yuan RY, Chen RM, Hu CJ (2009) The epigenetic effects of amyloid-beta(1-40) on global DNA and neprilysin genes in murine cerebral endothelial cells. *Biochem Biophys Res Commun* **378**, 57-61.

[12] Russo R, Borghi R, Markesbery W, Tabaton M, Piccini A (2005) Neprylisin decreases uniformly in Alzheimer's disease and in normal aging. *FEBS Lett* **579**, 6027-6030.

[13] Darst RP, Pardo CE, Ai L, Brown KD, Kladde MP (2010) Bisulfite sequencing of DNA. *Curr Protoc Mol Biol* **Chapter 7**, Unit 7 9 1-17.

[14] Raizis AM, Schmitt F, Jost JP (1995) A bisulfite method of 5-methylcytosine mapping that minimizes template degradation. *Anal Biochem* **226**, 161-166.

[15] Palmke N, Santacruz D, Walter J (2010) Comprehensive analysis of DNA-methylation in mammalian tissues using MeDIP-chip. *Methods*.

[16] Melnikov AA, Gartenhaus RB, Levenson AS, Motchoulskaia NA, Levenson Chernokhvostov VV (2005) MSRE-PCR for analysis of gene-specific DNA methylation. *Nucleic Acids Res* **33**, e93.

[17] Khulan B, Thompson RF, Ye K, Fazzari MJ, Suzuki M, Stasiek E, Figueroa ME, Glass JL, Chen Q, Montagna C, Hatchwell E, Selzer RR, Richmond TA, Green RD, Melnick A, Greally JM (2006) Comparative isoschizomer profiling of cytosine methylation: the HELP assay. *Genome Res* **16**, 1046-1055.

[18] Costello RW, Maloney M, Atiyeh M, Gleich G, Walsh MT (2011) Mechanism of sphingosine 1-phosphate- and lysophosphatidic Acid-induced up-regulation of adhesion molecules and eosinophil chemoattractant in nerve cells. *Int J Mol Sci* **12**, 3237-3249.

[19] Curran DR, Morgan RK, Kingham PJ, Durcan N, McLean WG, Walsh MT, Costello RW (2005) Mechanism of eosinophil induced signaling in cholinergic IMR-32 cells. *Am J Physiol Lung Cell Mol Physiol* **288**, L326-332.

[20] Oda M, Glass JL, Thompson RF, Mo Y, Olivier EN, Figueroa ME, Selzer RR, Richmond TA, Zhang X, Dannenberg L, Green RD, Melnick A, Hatchwell E, Bouhassira EE, Verma A, Suzuki M, Greally JM (2009) High-resolution genome-wide cytosine methylation profiling with simultaneous copy number analysis and optimization for limited cell numbers. *Nucleic Acids Res* **37**, 3829-3839.

[21] Suzuki M, Greally JM (2010) DNA methylation profiling using HpaII tiny fragment enrichment by ligation-mediated PCR (HELP). *Methods* **52**, 218-222.

[22] McLean CY, Bristor D, Hiller M, Clarke SL, Schaar BT, Lowe CB, Wenger AM, Bejerano G (2010) GREAT improves functional interpretation of cis-regulatory regions. *Nat Biotechnol* **28**, 495-501.

[23] Tabas-Madrid D, Nogales-Cadenas R, Pascual-Montano A (2012) GeneCodis3: a non-redundant and modular enrichment analysis tool for functional genomics. *Nucleic Acids Res* **40**, W478-483.

[24] Nogales-Cadenas R, Carmona-Saez P, Vazquez M, Vicente C, Yang X, Tirado F, Carazo JM, Pascual-Montano A (2009) GeneCodis: interpreting gene lists through enrichment analysis and integration of diverse biological information. *Nucleic Acids Res* **37**, W317-322.

[25] Carmona-Saez P, Chagoyen M, Tirado F, Carazo JM, Pascual-Montano A (2007) GENECODIS: a web-based tool for finding significant concurrent annotations in gene lists. *Genome Biol* **8**, R3.

[26] Kulaeva OI, Nizovtseva EV, Polikanov YS, Ulianov SV, Studitsky VM (2012) Distant activation of transcription: mechanisms of enhancer action. *Mol Cell Biol* **32**, 4892-4897.

[27] Marsman J, Horsfield JA (2012) Long distance relationships: enhancer-promoter communication and dynamic gene transcription. *Biochim Biophys Acta* **1819**, 1217-1227.

[28] Ehrlich M, Woods CB, Yu MC, Dubeau L, Yang F, Campan M, Weisenberger DJ, Long T, Youn B, Fiala ES, Laird PW (2006) Quantitative analysis of associations between DNA hypermethylation, hypomethylation, and DNMT RNA levels in ovarian tumors. *Oncogene* **25**, 2636-2645.

[29] Rauch TA, Zhong X, Wu X, Wang M, Kernstine KH, Wang Z, Riggs AD, Pfeifer GP (2008) High-resolution mapping of DNA hypermethylation and hypomethylation in lung cancer. *Proc Natl Acad Sci U S A* **105**, 252-257.

[30] Weisenberger DJ, Campan M, Long TI, Kim M, Woods C, Fiala E, Ehrlich M, Laird PW (2005) Analysis of repetitive element DNA methylation by MethyLight. *Nucleic Acids Res* **33**, 6823-6836.

[31] Cobos I, Borello U, Rubenstein JL (2007) Dlx transcription factors promote migration through repression of axon and dendrite growth. *Neuron* **54**, 873-888.

[32] Nyhan MJ, O'Sullivan GC, McKenna SL (2008) Role of the VHL (von Hippel-Lindau) gene in renal cancer: a multifunctional tumour suppressor. *Biochem Soc Trans* **36**, 472-478.

[33] Lee K, Rhee K (2011) PLK1 phosphorylation of pericentrin initiates centrosome maturation at the onset of mitosis. *J Cell Biol* **195**, 1093-1101.

[34] Wang Y, Dantas TJ, Lalor P, Dockery P, Morrison CG (2013) Promoter hijack reveals pericentrin functions in mitosis and the DNA damage response. *Cell Cycle* **12**, 635-646.

[35] Willems M, Genevieve D, Borck G, Baumann C, Baujat G, Bieth E, Edery P, Farra C, Gerard M, Heron D, Leheup B, Le Merrer M, Lyonnet S, Martin-Coignard D, Mathieu M, Thauvin-Robinet C, Verloes A, Colleaux L, Munnich A, Cormier-Daire V (2010) Molecular analysis of pericentrin gene (PCNT) in a series of 24 Seckel/microcephalic osteodysplastic primordial dwarfism type II (MOPD II) families. *J Med Genet* **47**, 797-802.

[36] De Larco JE, Wuertz BR, Yee D, Rickert BL, Furcht LT (2003) Atypical methylation of the interleukin-8 gene correlates strongly with the metastatic potential of breast carcinoma cells. *Proc Natl Acad Sci U S A* **100**, 13988-13993.

[37] Niesen MI, Osborne AR, Yang H, Rastogi S, Chellappan S, Cheng JQ, Boss JM, Blanck G (2005) Activation of a methylated promoter mediated by a sequence-specific DNA-binding protein, RFX. *J Biol Chem* **280**, 38914-38922.

[38] Unoki M, Nakamura Y (2003) Methylation at CpG islands in intron 1 of EGR2 confers enhancer-like activity. *FEBS Lett* **554**, 67-72.

[39] Yu DH, Ware C, Waterland RA, Zhang J, Chen MH, Gadkari M, Kunde-Ramamoorthy G, Nosavanh LM, Shen L (2013) Developmentally programmed 3' CpG island methylation confers tissue- and cell-type-specific transcriptional activation. *Mol Cell Biol* **33**, 1845-1858.

Figure Legends

Figure 1. Global DNA Methylation Distribution in Neurons Remains Largely Unchanged After Aβ Treatment *In Vitro*.

The $\log_2$ HpaII/MspI ratios for the control and Aβ-treated microarray probes are plotted as frequency distributions. The data are mean-centered at zero (vertical grey line), with negative ratios and positive ratios signifying loci more and less methylated than the mean level of methylation, respectively. The blue and red curves represent the two components of the bimodal distribution. Each curve shows the probability of the data of each bin belonging to the left peak or the right peak of these bimodal distributions. (A) The mean HpaII/MspI ratios of the blue and the red curve are -0.66 and 1.76, respectively. (B) The mean HpaII/MspI ratios of the blue and the red curve are -0.76 and 1.95, respectively.

Figure 2. Site-specific qPCR Confirms the Microarray Data.

The landscapes of microarray regions selected for confirmations are plotted with purple bars representing the probe values. Triangles represent the 5'-CCGG-3' sequences in those regions. The qPCR results for the chosen CCGGs (red triangles) are generated by setting the 2^(-(Cq)) of the MspI-digested DNA qPCR curve to "1" and setting the HpaII bar to represent the value of $2^{(-(Cq_{HpaII}-Cq_{MspI}))}$.

Figure 3. Aβ Induces High Changes in Methylation Levels in a Subset of Loci.

The data from the control microarray were subtracted from the Aβ-treated microarray data, and the result is plotted as a frequency distribution. The two dashed boxes represent the "upper" and "lower" 0.05% regions of all changing regions. A close-up frequency distribution of the "lower" 0.05% of the probes with the highest decrease in HpaII/MspI ratio (B) and a close-up frequency

distribution of the "upper" 0.05% of the probes with the highest increase in HpaII/MspI ratio (C) are shown.

Figure 4. Aβ-induced Probe Ratio Changes Correspond to CpG Methylation Changes.

The landscapes of microarray regions selected for confirmations are plotted with purple bars representing the (Aβ - control) value for the probes. Triangles represent the 5'-CCGG-3' sequences mapped to the region, with red triangles showing the specific CCGG sequences selected for qPCR analysis. Two separate sequences were chosen per region, one upstream and one downstream of the greatest changing probe. The "none" and "Aβ" bars in the qPCR graphs represent the value of $2^{(-(Cq_{HpaII}-Cq_{MspI}))}$ in the control and Aβ sample DNA, respectively.

Figure 5. Methylation Changes Occur at Promoter Proximal and Distal Regions.

The microarray landscapes for two genes associated with neuronal differentiation (DLX1) and cell division (VHL) are shown. The landscapes demonstrate that Aβ-induced methylation changes can occur at regions proximal (VHL) or distal (DLX1) to the TSS (illustrated by a green arrow). Note that the x-axis has breaks to eliminate genomic gaps that do not contain probe data.

Figure 6. An Epigenetic Model of Aβ Pathology.

DLX1 protein is involved in repressing the dendrite and axon growth of neurons, preventing differentiation. By decreasing the methylation at DLX1, Aβ can increase the activity of this gene and promote the de-differentiation of mature neurons. Aβ also decreases the methylation near the VHL TSS, and increases methylation near the PCNT TSS; this consequently alters the expression profile of these genes. Given that VHL is a tumor suppressor and PCNT is a director of mitotic spindle assembly, such methylation changes may eventually prevent neuronal precursor cells (NPCs) from dividing and replacing the damaged cells. Put together, these

alterations decrease the number of functional neurons and may eventually result in the loss of memory and brain mass seen in Alzheimer's disease.

Supplemental Figure Legends

Supplemental Figure 1. Correlation of HpaII/MspI Ratios from Control IMR-32 Cells

A scatter-plot of the probe ratios is shown comparing the microarray data from the individual control (untreated) replicates. The correlation coefficient was calculated using MatLab.

Supplemental Figure 2. QPCR Confirmation of Regions with an Aβ-induced Methylation Increase

Regions selected for ontological examination were randomly selected and subjected to qPCR analysis using differential enzyme digestion. The HpaII/MspI ratios were determined with higher ratios demonstrating a reduction in HpaII cutting efficiency. Higher ratios reflect an increase in 5'-CCGG-3' methylation and an increase in protection from HpaII digestion. The white and black bars in the qPCR graph represent the $\log_{10}$ value of $2^{(-(Cq_{HpaII}-Cq_{MspI}))}$ in the control and Aβ sample DNA, respectively. Each region (X-axis) was analyzed twice using different primer sets as indicated by the two sets of bars per region. An asterisk indicates a region of study where the qPCR primers failed to work.

Supplemental Figure 3. QPCR Confirmation of Regions with an Aβ-induced Methylation Decrease

Regions selected for ontological examination were randomly selected and subjected to qPCR analysis using differential enzyme digestion. The HpaII/MspI ratios were determined with lower ratios demonstrating an increase in HpaII cutting efficiency. Lower ratios reflect an decrease in 5'-CCGG-3' methylation and a decrease in protection from HpaII digestion. The white and black bars in the qPCR graph represent the $\log_{10}$ value of $2^{(-(Cq_{HpaII}-Cq_{MspI}))}$ in the control and Aβ sample DNA, respectively. Each region (X-axis) was analyzed twice using different primer sets as indicated by the two sets of bars per region. An asterisk indicates a region of study where the

qPCR primers failed to work. One region had a 5'-CCGG-3' sequence that did not show a methylation decrease (indicated by a †).

Supplemental Figure 4. Relative Gene Locations of Regions with Aβ-induced Methylation Changes

The genomic regions with the greatest Aβ-induced methylation change were analyzed by GREAT to determine the distance to the transcription start site of nearby genes. A histogram of that distribution is shown with each bar representing the number of regions increasing (yellow) or decreasing (blue) their methylation status upon Aβ treatment.

Supplemental Table 1. Significantly Changing Regions and Their Relative Distance from Nearby Genes

An excel sheet of the GREAT output file is given showing the association of each genomic region to a specific gene symbol. The relative distance from the center of each genomic region to a nearby transcription start site (TSS) is shown in parenthesis. The methylation status change (loss or gain) is also indicated.

Figure 1. Global DNA Methylation Levels Remain Largely Unchanged After Aβ Treatment.

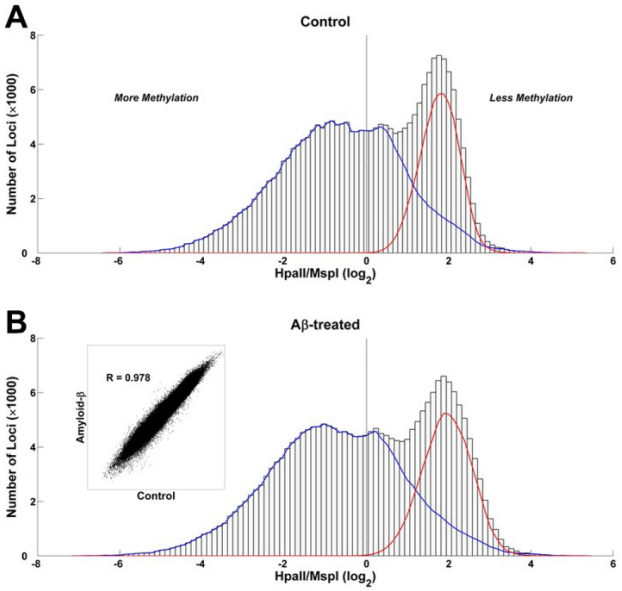

Figure 2. Site-specific qPCR Confirms the Microarray Data.

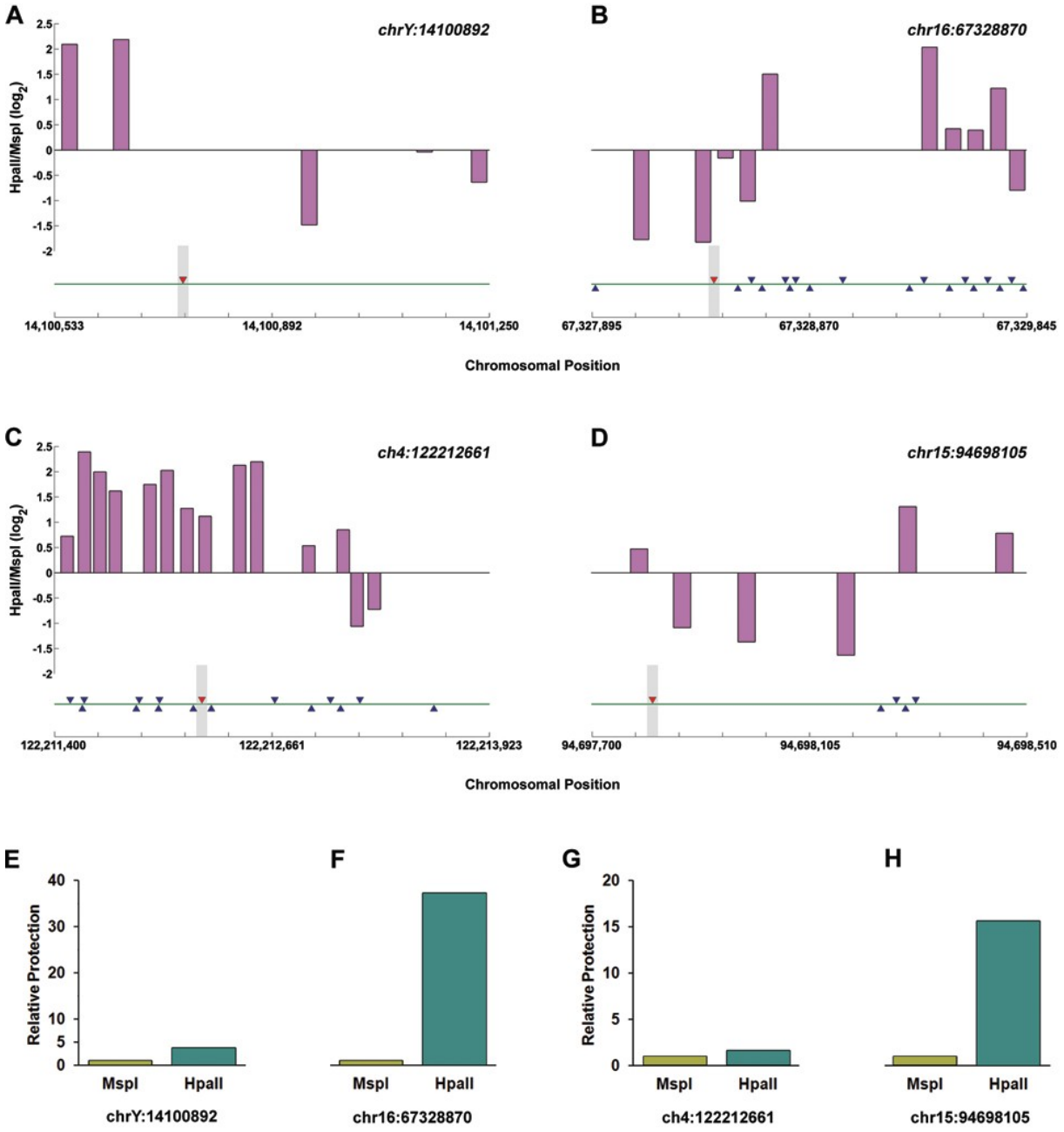

Figure 3. Aβ Induces Significant Changes in DNA Methylation at a Subset of Genomic Locations.

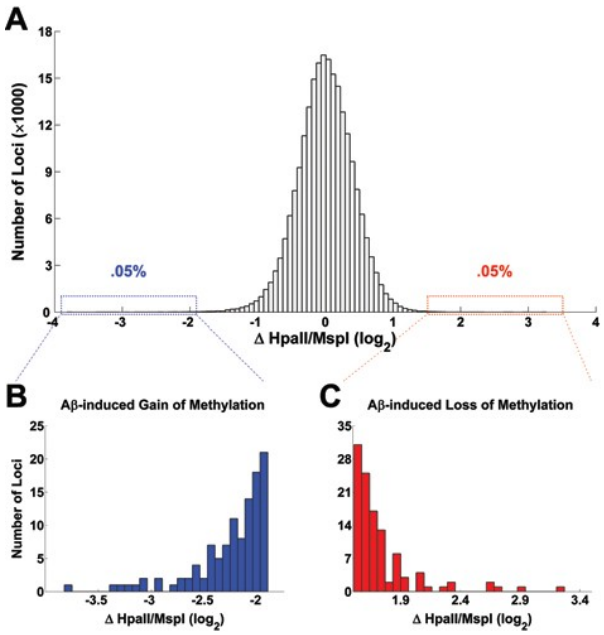

Figure 4. Aβ-induced Probe Ratio Changes Correspond to CpG Methylation Changes.

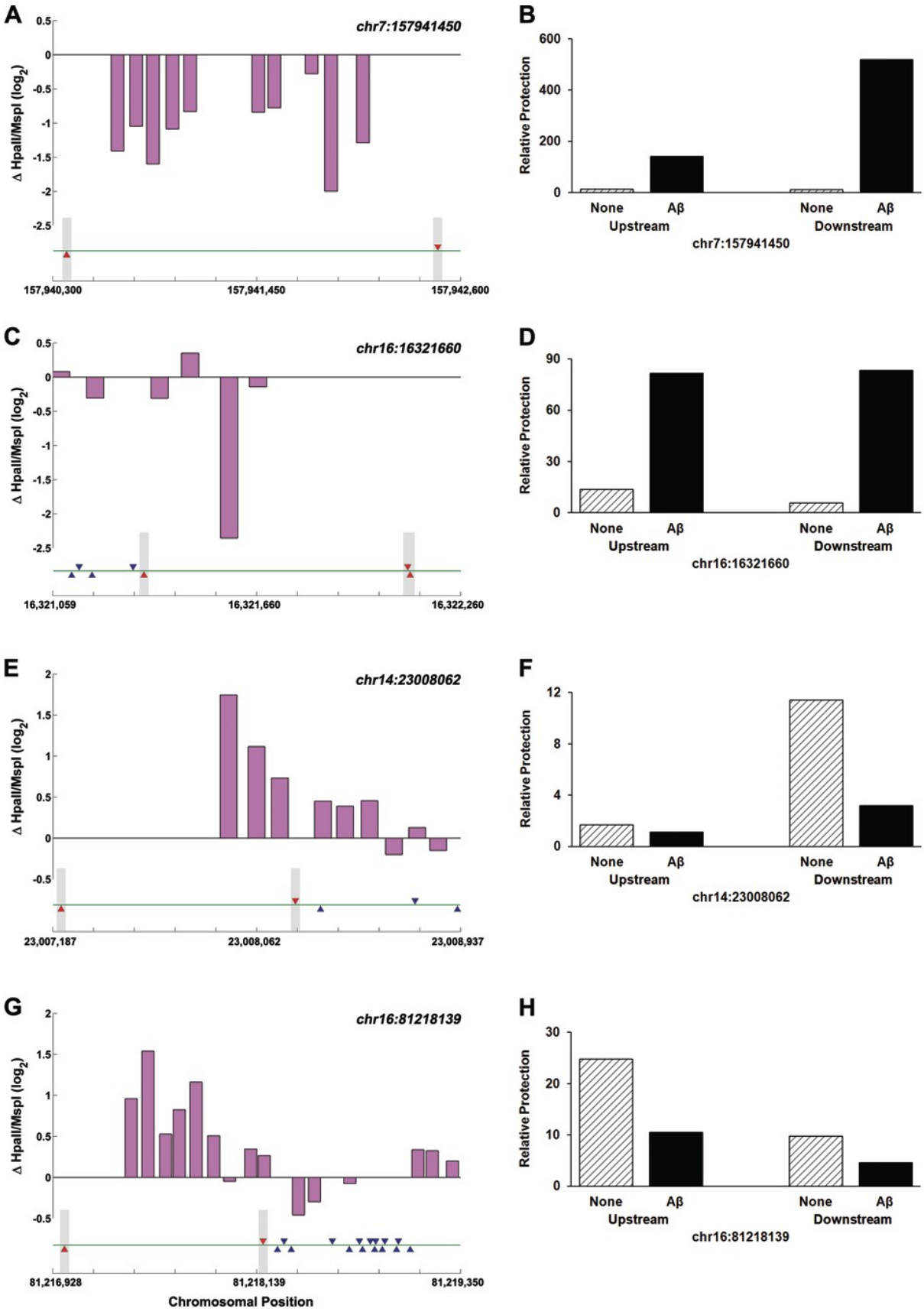
A
chr7:157941450
Δ HpaII/MspI (log2)
157,940,300
157,941,450
157,942,600
B
Relative Protection
None
Aβ
Upstream
Downstream
chr7:157941450
C
chr16:16321660
16,321,059
16,321,660
16,322,260
D
chr16:16321660
E
chr14:23008062
23,007,187
23,008,062
23,008,937
F
chr14:23008062
G
chr16:81218139
81,216,928
81,218,139
81,219,350
Chromosomal Position
H
chr16:81218139

Table 1. Aβ Alters the DNA Methylation of Cell Fate Genes.

Gene Set	Gene Ontology[a]	Genes[b]	p-value[c]	Enrichment
Genes Becoming Hypomethylated (107 Genes)	Regulation of Neurogenesis; CNS Neuron Differentiation	DLX1, DLX2	0*	192
	Neurogenesis; CNS Development	SOX9, NKX6-2	1.87×10^{-43}	61
	Regulation of Nervous System Development	MBP, ACCN1	1.02×10^{-21}	38
	Negative Regulation of Apoptotic Process	VHL, HAND2	1.91×10^{-17}	30
Genes Becoming Hypermethylated (77 Genes)	Brain Development	PCNT, SKI	1.66×10^{-16}	29
	Regulation of Apoptotic Process	GAS6, LYST, ADAM8	2.03×10^{-10}	18
	Neurogenesis	DLL1, MAPK8IP3	7.89×10^{-10}	13
Random[d] (143 Genes)	None		$>9 \times 10^{-7}$	NA

[a] Only ontologies that were considered relevant to the study are listed.

[b] Genes found in several ontologies are not listed multiple times for clarity purposes.

[c] The p-value for each gene set-ontology association was determined by GeneCodis using Chi-square tests.

[d] A random list of regions was generated using MATLAB. This list was subjected to the same analysis as the list containing the changing regions. No gene ontologies were enriched to the same degree as the lowest ontology enrichment from the specific list.

* The gene ontology p-value was displayed as zero due to limitations in the calculation input. The value was too low to be successfully determined, which suggests that it is $<1.87 \times 10^{-43}$ due to this p-value being successfully calculated.

Figure 5. Methylation Changes Occur at Promoter-proximal and Distal Regions.

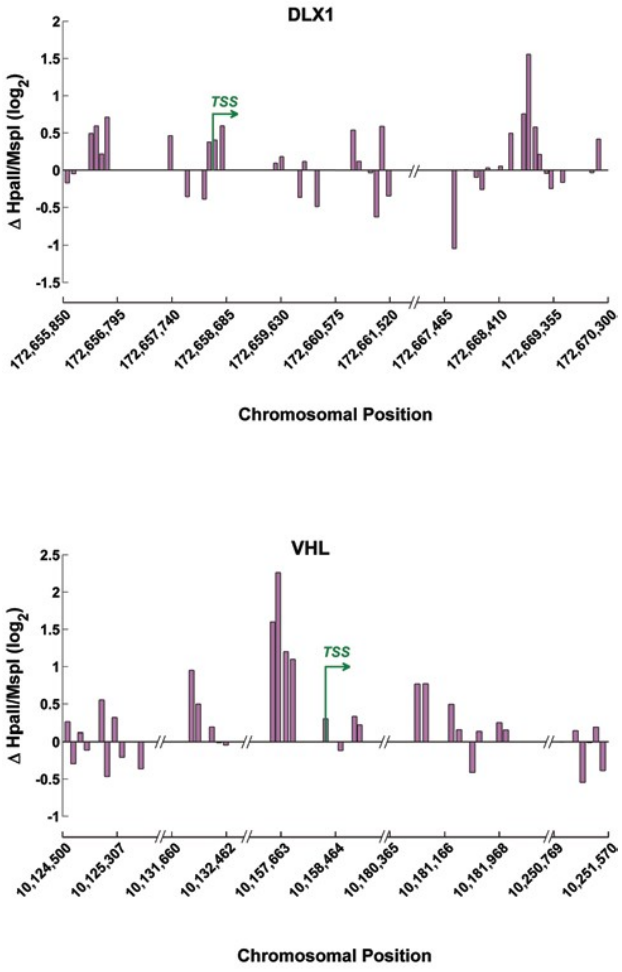

Figure 6. An Epigenetic Model of Aβ Pathology

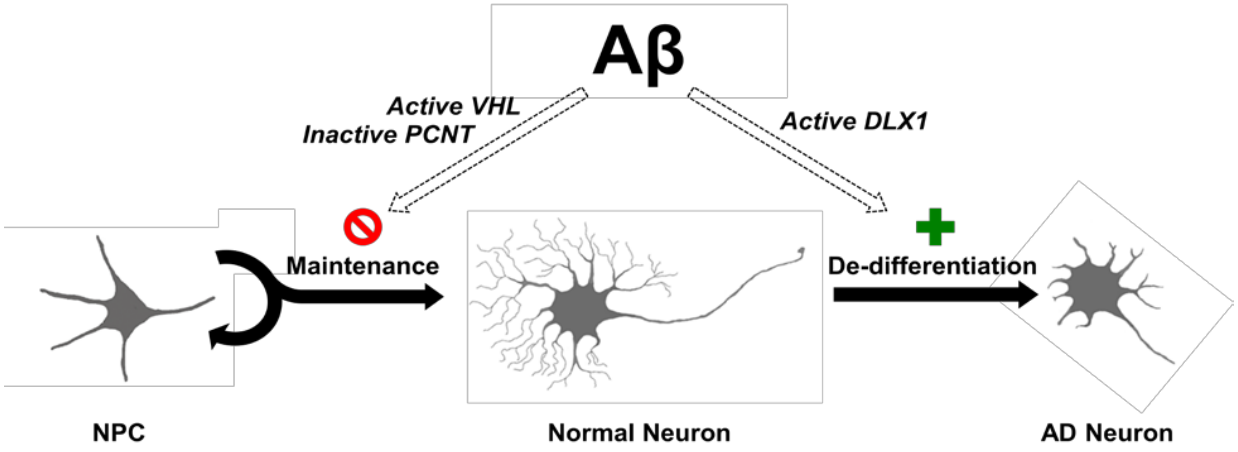

Supplemental Figure 1. Correlation of HpaII/MspI Ratios from Control IMR-32 Cells

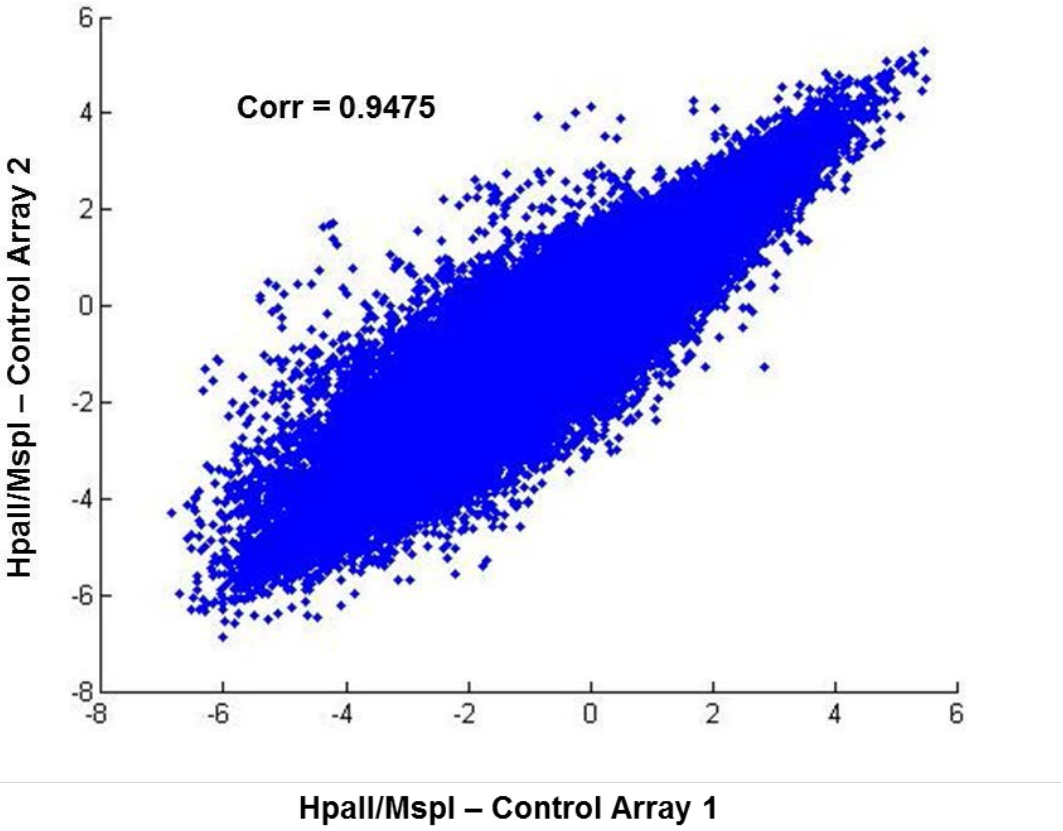

Supplemental Figure 2. QPCR Confirmation of Regions with an Aβ-Induced Methylation Increase

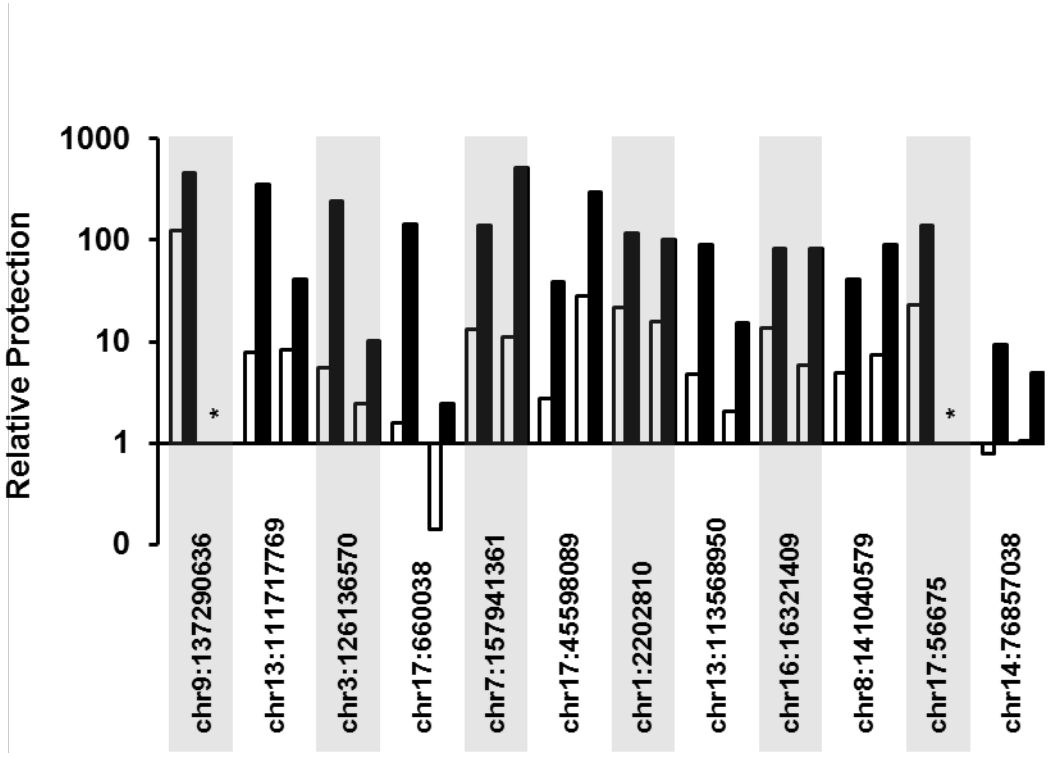

Supplemental Figure 3. QPCR Confirmation of Regions with an AB-Induced Methylation Decrease

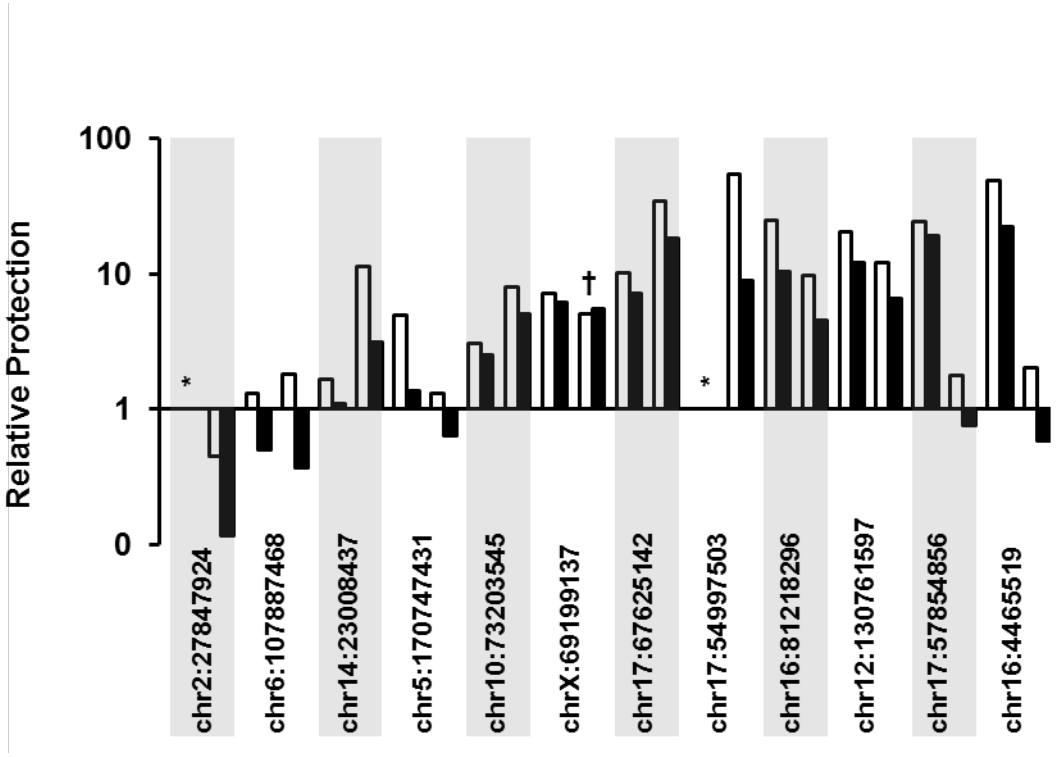

Supplemental Figure 4. Relative Gene Locations of Regions with Aβ-Induced Methylation Changes.

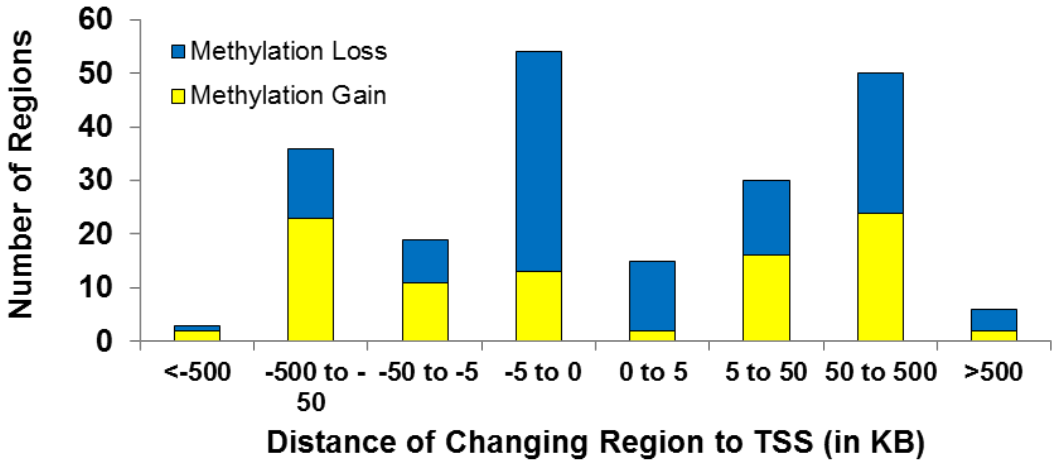

Supplemental Table 1. Significantly Changing Regions and Their Relative Distance from Nearby Genes

Gene Symbol	Changing Region (distance to TSS)	Aβ-induced Change
ABCC5	chr3:185217681-185219221 (-30)	Loss of methylation
ABCG1	chr21:42527874-42528575 (+15889)	Loss of methylation
ABHD6	chr3:58197548-58199404 (+177)	Loss of methylation
ACCN1	chr17:29507738-29508738 (-300)	Loss of methylation
ACP6	chr1:145608466-145610038 (+6)	Loss of methylation
ANKLE2	chr12:131806082-131806782 (+42092)	Loss of methylation
ANO10	chr3:43637980-43639364 (-108)	Loss of methylation
ARFGAP2	chr11:46914026-46915276 (+240344)	Loss of methylation
ARID3A	chr19:934527-935866 (+58160)	Loss of methylation
ASPSCR1	chr17:77545256-77546605 (+17216)	Loss of methylation
ATRIP	chr3:48462421-48463585 (-219)	Loss of methylation
AWAT2	chrX:69198265-69200010 (-12625)	Loss of methylation
C10orf54	chr10:73202947-73204143 (-202)	Loss of methylation
C18orf62	chr18:71128507-71129207 (+139720)	Loss of methylation
C19orf29	chr19:3648693-3649393 (-71230)	Loss of methylation
C1QTNF8	chr16:1082316-1084088 (+3043)	Loss of methylation
C8orf30A	chr8:145407887-145409553 (+32)	Loss of methylation
CDH13	chr16:81217278-81219314 (+217)	Loss of methylation
CEBPG	chr19:38555648-38556850 (-200)	Loss of methylation
CENPJ	chr13:24394588-24395818 (-118)	Loss of methylation
CMTM1	chr16:65156996-65158350 (-178)	Loss of methylation
DACT2	chr6:168513887-168514588 (-50987)	Loss of methylation
DHX40	chr17:54996867-54998139 (-165)	Loss of methylation
DIO3	chr14:100419019-100419719 (-678072)	Loss of methylation
DLX1	chr2:172667513-172670300 (+10453)	Loss of methylation
DLX2	chr2:172667513-172670300 (+6817)	Loss of methylation
E2F4	chr16:65782768-65783768 (-301)	Loss of methylation
EBF3	chr10:131576120-131576820 (+75611)	Loss of methylation
EIF4G1	chr3:185514249-185515987 (-547)	Loss of methylation
EPN3	chr17:45968821-45969521 (+4124)	Loss of methylation
EXOC3L	chr16:65782768-65783768 (-1660)	Loss of methylation
F11	chr4:187529470-187530572 (+105909)	Loss of methylation
FAM18B2	chr17:15406976-15408370 (-103)	Loss of methylation
FLJ43860	chr8:142839591-142840292 (-253430)	Loss of methylation
FUBP3	chr9:132443980-132445317 (-132)	Loss of methylation
GLS2	chr12:55167668-55169248 (-10)	Loss of methylation
GLTP	chr12:108767404-108768105 (+34921)	Loss of methylation

GRIN3B	chr19:934527-935866 (-16240)	Loss of methylation
HAND1	chr5:154006880-154007581 (-169214)	Loss of methylation
HAND2	chr4:174664266-174664967 (+23336)	Loss of methylation
HMOX2	chr16:4464076-4466962 (-823)	Loss of methylation
HOXB5	chr17:44025521-44026902 (-110)	Loss of methylation
IFT140	chr16:1597101-1598101 (-302)	Loss of methylation
IGBP1	chrX:69198265-69200010 (-70905)	Loss of methylation
ING4	chr12:6642329-6643365 (-278)	Loss of methylation
INPP5A	chr10:134354410-134355581 (+153653)	Loss of methylation
IQSEC1	chr3:12924512-12925212 (+59098)	Loss of methylation
IQSEC2	chrX:53300308-53301009 (+66588)	Loss of methylation
JARID1C	chrX:53300308-53301009 (-29330)	Loss of methylation
JHDM1D	chr7:139638566-139639267 (-115707)	Loss of methylation
KCNQ1	chr11:1699992-3143916 (-843)	Loss of methylation
KDELC2	chr11:107873708-107875121 (-46)	Loss of methylation
KIAA1890	chr8:2325222-2325923 (+928962)	Loss of methylation
LARP1	chr5:154006880-154007581 (-107851)	Loss of methylation
LDHC	chr11:18389628-18390682 (-279)	Loss of methylation
LRP4	chr11:46914026-46915276 (-17999)	Loss of methylation
MBP	chr18:72820002-72820702 (+153410)	Loss of methylation
METTL2A	chr17:57854197-57855516 (-121)	Loss of methylation
MGMT	chr10:131576120-131576820 (+421014)	Loss of methylation
MKRN1	chr7:139824758-139826571 (+106)	Loss of methylation
MRPL33	chr2:27847287-27848561 (-164)	Loss of methylation
MTNR1A	chr4:187529470-187530572 (+183510)	Loss of methylation
MYOM2	chr8:2325222-2325923 (+345008)	Loss of methylation
MYOM2	chr8:2173367-2174068 (+193153)	Loss of methylation
NGDN	chr14:23007937-23008937 (-301)	Loss of methylation
NKX6-2	chr10:134354410-134355581 (+94531)	Loss of methylation
NMB	chr15:82977632-82978418 (+24781)	Loss of methylation
NMRAL1	chr16:4464076-4466962 (-622)	Loss of methylation
NPM1	chr5:170746602-170748260 (+28)	Loss of methylation
OR10J5	chr1:157772221-157773221 (-300)	Loss of methylation
OR11H1	chr22:14608025-14608726 (+221428)	Loss of methylation
PCBP3	chr21:45877482-45878832 (-216146)	Loss of methylation
PDSS2	chr6:107886688-107888248 (+4)	Loss of methylation
PGAM5	chr12:131806082-131806782 (+8923)	Loss of methylation
PIAS1	chr15:66132825-66134462 (+18)	Loss of methylation
PIP5K1C	chr19:3648693-3649393 (+2402)	Loss of methylation
PRPF4B	chr6:3965767-3967073 (-148)	Loss of methylation
PSMF1	chr20:1046444-1047670 (-183)	Loss of methylation
RCN1	chr11:32068466-32069853 (-107)	Loss of methylation
RIMBP2	chr12:129691556-129692257 (-123492)	Loss of methylation

RP1L1	chr8:10486075-10486775 (+63602)	Loss of methylation
RPL32	chr3:12924512-12925212 (-67913)	Loss of methylation
SAP18	chr13:20611884-20613115 (-185)	Loss of methylation
SCAND2	chr15:82977632-82978418 (+2330)	Loss of methylation
SCRG1	chr4:174664266-174664967 (-107425)	Loss of methylation
SFRS8	chr12:130760787-130762407 (+9)	Loss of methylation
SH2D3C	chr9:129573138-129574172 (+7078)	Loss of methylation
SLC19A1	chr21:45877482-45878832 (-91378)	Loss of methylation
SLC37A3	chr7:139638566-139639267 (+105863)	Loss of methylation
SMOC2	chr6:168513887-168514588 (-70642)	Loss of methylation
SMOC2	chr6:168679057-168679757 (+94527)	Loss of methylation
SMOC2	chr6:169166157-169167446 (+581922)	Loss of methylation
SOX9	chr17:67624419-67625866 (-3613)	Loss of methylation
SPAG8	chr9:35801889-35803059 (-215)	Loss of methylation
SPARCL1	chr4:88669330-88670330 (-151)	Loss of methylation
SPATA20	chr17:45968821-45969521 (-10257)	Loss of methylation
SSTR5	chr16:1082316-1084088 (+14332)	Loss of methylation
STRA13	chr17:77545256-77546605 (+28131)	Loss of methylation
STX2	chr12:129691556-129692257 (+197857)	Loss of methylation
TAF10	chr11:6589455-6590821 (-117)	Loss of methylation
TFF3	chr21:42527874-42528575 (+80550)	Loss of methylation
THBS2	chr6:168679057-168679757 (+716655)	Loss of methylation
THBS2	chr6:169166157-169167446 (+229260)	Loss of methylation
TMEM131	chr2:97716500-97717903 (+261584)	Loss of methylation
TOR2A	chr9:129573138-129574172 (-36230)	Loss of methylation
TRPV4	chr12:108767404-108768105 (-12160)	Loss of methylation
TSHZ1	chr18:71128507-71129207 (+77138)	Loss of methylation
TSNARE1	chr8:142839591-142840292 (+642502)	Loss of methylation
TTC15	chr2:3361652-3363020 (-117)	Loss of methylation
UNQ9391	chr8:10486075-10486775 (+65934)	Loss of methylation
UQCC	chr20:33463047-33464047 (-300)	Loss of methylation
VHL	chr3:10157518-10158973 (-73)	Loss of methylation
YDJC	chr22:20316285-20317285 (-2445)	Loss of methylation
ZAP70	chr2:97716500-97717903 (+20739)	Loss of methylation
ZFP36L1	chr14:68332743-68333743 (-3705)	Loss of methylation
ZNF195	chr11:3356513-3357691 (-111)	Loss of methylation
ZNF236	chr18:72820002-72820702 (+155248)	Loss of methylation
ZNF556	chr19:2839720-2840421 (+21738)	Loss of methylation
ZNF57	chr19:2839720-2840421 (-11893)	Loss of methylation
hCG_25025	chr14:100419019-100419719 (+51858)	Loss of methylation
AADAC	chr3:153013750-153014750 (-301)	Gain of methylation
ADAM8	chr10:134948526-134949226 (-8514)	Gain of methylation
ADK	chr10:75605649-75606828 (+25268)	Gain of methylation

BATF3	chr1:210939083-210940750 (+33)	Gain of methylation
BEND7	chr10:13556112-13556812 (+28520)	Gain of methylation
BEND7	chr10:13553694-13554394 (+30938)	Gain of methylation
BEND7	chr10:13554962-13555662 (+29670)	Gain of methylation
C10orf93	chr10:134726320-134728529 (-121371)	Gain of methylation
C13orf16	chr13:111717249-111718290 (+946754)	Gain of methylation
C13orf28	chr13:111865817-111866940 (-212291)	Gain of methylation
C13orf3	chr13:20849155-20849855 (-200795)	Gain of methylation
C14orf180	chr14:103966949-103968654 (-149299)	Gain of methylation
C5orf45	chr5:179209213-179209913 (+8883)	Gain of methylation
C6orf70	chr6:170295849-170296860 (+402709)	Gain of methylation
C6orf89	chr6:36960817-36962087 (-166)	Gain of methylation
C8orf42	chr8:1250830-1253745 (-766957)	Gain of methylation
COMT	chr22:18274383-18275428 (-34403)	Gain of methylation
DIP2A	chr21:46626893-46629188 (-75277)	Gain of methylation
DLGAP2	chr8:1250830-1253745 (-184688)	Gain of methylation
DLL1	chr6:170295849-170296860 (+145267)	Gain of methylation
EXOC2	chr6:464079-466338 (+172900)	Gain of methylation
FAM70B	chr13:113568450-113569450 (+82923)	Gain of methylation
GALNT2	chr1:228534950-228535650 (+265649)	Gain of methylation
GAS6	chr13:113568450-113569450 (+22037)	Gain of methylation
GLOD4	chr17:659688-660388 (-27741)	Gain of methylation
GNB1L	chr22:18274383-18275428 (-52444)	Gain of methylation
GPR123	chr10:134726320-134728529 (-6998)	Gain of methylation
GPR133	chr12:129937778-129938478 (-66277)	Gain of methylation
GPR133	chr12:130736641-130737341 (+732586)	Gain of methylation
GRIP1	chr12:65358820-65359820 (-300)	Gain of methylation
GSTZ1	chr14:76856306-76857770 (-69)	Gain of methylation
GTPBP6	chrY:243871-244571 (-73334)	Gain of methylation
GTPBP6	chrX:243871-244571 (-73334)	Gain of methylation
IGF2R	chr6:160309320-160447571 (+68325)	Gain of methylation
INPP5A	chr10:134154101-134154801 (-46892)	Gain of methylation
IRF4	chr6:464079-466338 (+128457)	Gain of methylation
KCNK9	chr8:141040229-141040929 (-256098)	Gain of methylation
KCNQ1	chr11:1699992-3143916 (-843)	Gain of methylation
KIAA0649	chr9:137290223-137291050 (-220832)	Gain of methylation
KIF26A	chr14:103966949-103968654 (+292989)	Gain of methylation
KLF6	chr10:3490104-3490804 (+327001)	Gain of methylation
LOC339047	chr16:16321059-16321760 (-11802)	Gain of methylation
LYST	chr1:234113363-234114363 (-17020)	Gain of methylation
MAPK8IP3	chr16:1730186-1730887 (+34315)	Gain of methylation
METTL11A	chr9:131290223-131290924 (-137682)	Gain of methylation
MFSD10	chr4:2926463-2927164 (-21247)	Gain of methylation

MUC13	chr3:126136070-126137070 (-300)	Gain of methylation
MYST4	chr10:75605649-75606828 (-650146)	Gain of methylation
MYT1	chr20:62280214-62280915 (+14294)	Gain of methylation
NID1	chr1:234113363-234114363 (+181241)	Gain of methylation
NME3	chr16:1730186-1730887 (+31174)	Gain of methylation
NOMO3	chr16:16321059-16321760 (+87520)	Gain of methylation
NOP14	chr4:2926463-2927164 (+8102)	Gain of methylation
NXN	chr17:659688-660388 (+169722)	Gain of methylation
OLFM1	chr9:137290223-137291050 (+183727)	Gain of methylation
PCMTD2	chr20:62280214-62280915 (-76927)	Gain of methylation
PCNT	chr21:46626893-46629188 (+59577)	Gain of methylation
PGBD5	chr1:228534950-228535650 (+44690)	Gain of methylation
PITRM1	chr10:3490104-3490804 (-285451)	Gain of methylation
POMT2	chr14:76856306-76857770 (-68)	Gain of methylation
PPP2R3B	chrX:243871-244571 (+23406)	Gain of methylation
PPP2R3B	chrY:243871-244571 (+23406)	Gain of methylation
PPP2R4	chr9:131290223-131290924 (+377509)	Gain of methylation
PTPRN2	chr7:157940649-157942073 (+131818)	Gain of methylation
RAN	chr12:129937778-129938478 (+15607)	Gain of methylation
RER1	chr1:2201880-2203741 (-110263)	Gain of methylation
RPH3AL	chr17:56119-57232 (+145900)	Gain of methylation
RPH3AL	chr17:252659-254674 (-51091)	Gain of methylation
SEPHS1	chr10:13556112-13556812 (-126176)	Gain of methylation
SEPHS1	chr10:13554962-13555662 (-125026)	Gain of methylation
SEPHS1	chr10:13553694-13554394 (-123758)	Gain of methylation
SFRS8	chr12:130736641-130737341 (-24597)	Gain of methylation
SGCA	chr17:45597589-45598589 (-301)	Gain of methylation
SKI	chr1:2201880-2203741 (+52817)	Gain of methylation
SLC22A1	chr6:160309320-160447571 (-84407)	Gain of methylation
SLC45A2	chr5:34020337-34021337 (-300)	Gain of methylation
SMEK2	chr2:55697771-55699053 (+205)	Gain of methylation
SMOC2	chr6:169051742-169052507 (+467245)	Gain of methylation
SOX1	chr13:111865817-111866940 (+96465)	Gain of methylation
SOX1	chr13:111717249-111718290 (-52144)	Gain of methylation
SPPL2B	chr19:2298135-2300732 (+19805)	Gain of methylation
SQSTM1	chr5:179209213-179209913 (+29115)	Gain of methylation
STK32C	chr10:134154101-134154801 (-182984)	Gain of methylation
TAF1A	chr1:220829418-220830678 (-170)	Gain of methylation
THBS2	chr6:169051742-169052507 (+343937)	Gain of methylation
TMPRSS9	chr19:2298135-2300732 (-41350)	Gain of methylation
TNRC4	chr1:149960410-149961111 (-4847)	Gain of methylation
TRAPPC9	chr8:141040229-141040929 (+497281)	Gain of methylation
TTC32	chr2:19964485-19966025 (-30)	Gain of methylation

VPS53	chr17:252659-254674 (+311179)	Gain of methylation
ZDHHC20	chr13:20849155-20849855 (+81918)	Gain of methylation
ZDHHC23	chr3:115148637-115150077 (-81)	Gain of methylation
ZNF511	chr10:134948526-134949226 (-23537)	Gain of methylation